IEEE Access
Multidisciplinary | Rapid Review | Open Access Journal

Received September 14, 2020, accepted September 18, 2020, date of publication September 24, 2020,
date of current version October 23, 2020.

Digital Object Identifier 10.1109/ACCESS.2020.3026333

A Miniature Robotic Turtle With Target Tracking and Wireless Charging Systems Based on IPMCs

QIMENG SUN, (Member, IEEE), JINZHE HAN, HUI LI, (Senior Member, IEEE), SHENG LIU, (Fellow, IEEE), SHENGNAN SHEN, (Senior Member, IEEE), YUNFAN ZHANG, (Member, IEEE), AND JIAZHENG SHENG
School of Power and Mechanical Engineering, Wuhan University, Wuhan 430072, China

Corresponding author: Hui Li (li_hui@whu.edu.cn)

This work was supported in part by the National Key Research and Development Program of China under Grant 2019YFB1704600, and in part by the Hubei Provincial Natural Science Foundation of China under Grant 2020CFA032.

ABSTRACT State-of-the-art autonomous micro-robotic turtles suffer from various limitations, such as power restrictions that minimize their deployment times. In this paper, an Ionic Polymer Metal Composite (IPMC) actuator-based centimeter-level biomimetic underwater robot was designed and developed as a robotic turtle with self-charging capabilities to overcome such limitations. It could move forward and make turns driven by five IPMCs on the water. The underwater charging station was able to transmit wideband ultrasonic and electromagnetic fields for electromagnetic induction charging. An ultrasonic communication system with one ultrasonic transmitter and two ultrasonic receivers was first fabricated to implement communication between the underwater station and the biomimetic underwater robot for autonomous tracking and rechargeable capabilities. Experiments were carried out to confirm the operation of the biomimetic underwater robot, which verified the centimeter-level rechargeable capabilities and autonomous target tracking features. The micro-robot demonstrated a self-tracking radial displacement error of approximately 6 mm and a charging reliability rate of more than 73%.

INDEX TERMS Microactuators, unmanned underwater vehicles, biomimetics, wireless power transmission.

I. INTRODUCTION

Developing underwater technologies for studying and maintaining the oceans has long been the subject of intense research [1], [2]. Marine robotics, in particular, have been an essential advancement, owing to the increased demands of oceanographic engineering. An important requirement of underwater robots is the ability to provide appropriate movements for the prescribed operating conditions under specific environmental limitations [3]. In addition, to ensure that the robots imitate the movement of aquatic animals, a biomimetic approach is often undertaken.

Researchers have attempted to fabricate underwater robots by assembling multiple traditional actuators, motors, and hinges to achieve the required movements based on biomimetic designs and analyses [4]. Many robots have also been developed using different actuators [5]–[8]. Although some robots have performed respectably, they are often too large and bulky, as they require multiple actuators or other additional parts to meet the strict design requirements.

Biomimetic underwater robots with smart actuators have received increasing attention from researchers, owing to their versatility and complex movements [9]. Most of these smart actuators are electrically driven, such as Ionic Polymer Metal Composites (IPMC) [10] and IPMC actuators [11]–[13]. However, these actuators often operate with low force and torque, which limit the weight and size of the biomimetic robots. If there is no wireless charging robot, when charging by wire, there will be the possibility of poor sealing due to plugging and pulling the sealing cover of charging port for many times.

IPMC actuator-based centimeter-level biomimetic underwater robots (see, e.g., [14], [15]) have been previously designed and fabricated with the ability of rechargeable capabilities [16]. Tan *et al.* [17], Chen *et al.* [18], Aureli *et al.* [19] and Chang and Kim [20] have reported autonomous swimming fish driven by IPMC. In recent years, wireless information interaction of location has

The associate editor coordinating the review of this manuscript and approving it for publication was Hamid Mohammad-Sedighi.

attracted researchers' attention. For example, Li and Guo [21], Li *et al.* [22] developed a father-son robot system using LEDs (light-emitting diodes) to send signals to control the motions of a microrobot, whereas Gao and Guo [23] developed a mother-son robot system using an infrared sensor that enabled communication between the microrobot and a mother submarine. Chen *et al.* [24] and Katzschmann *et al.* [25] adopted acoustic communication method for information interaction of location. Wang and Xie [26] used visual and inertial cues to realize online high-precision probabilistic localization of robotic fish. Researchers have also studied the wireless rechargeable capabilities of marine robots, which would increase the practicality of these technologies. Itoh *et al.* [27] and Abdelnour *et al.* [28] investigated the magnetic-resonance-based wireless charging of underwater robots. Phamduy *et al.* [29] studied the docking and autonomous wireless charging of robotic fish, but they did not mention how long the underwater robot could work and how far it could swim without charging.

In this paper, we designed a miniature robotic turtle with target tracking and wireless charging system to overcome the limitations of previously reported systems. Its tracking and wireless charging performances were evaluated.

The paper is organized as follows. The design of the miniature robotic turtle with target tracking and wireless charging systems is detailed in Section II. Performance evaluations of key components are presented in Section III. Evaluations of the target tracking and wireless charging system are presented in Section IV. Finally, the conclusions and future work are provided in Section V.

II. SYSTEM DESIGN

The robotic turtle is designed to be fully autonomous, which consists of a packaged body and five IPMC fins (four pectoral fins and one caudal fin). The wires for the IPMC extend from the electronic device to the electrodes through the waterproof shell. Two electrodes are used to provide electrical signals for the IPMC in water. Five small rubber rings are used to fasten the IPMC and PVC (polyvinyl chloride) fins to a cantilever structure for swinging. Under normal operating conditions (applied voltage of 1∼25 V), there is no interference with propulsion when electrolysis occurs at the electrode position. The battery and the electronic device for signal controlling and outputting are packaged in a shell made of waterproof latex.

The physical data of the robot are as follows: 9.5 cm in length (6 cm excluding the tail fin) and 30 g in weight. The robot is designed with the ability to go straight, turn left, or turn right (Fig. 1). Fig. 2 shows the onboard electronics of the robotic turtle system. Internal parts of waterproof shell include the micro-controller, charging circuit, manostat rectifier, coil 2 and battery. External parts of the shell include the IPMCs with the PVCs and two ultrasonic receivers. The charging station includes the power, coil 1 and ultrasonic transmitter. The key specifications of the robotic turtle are listed in Table 1.

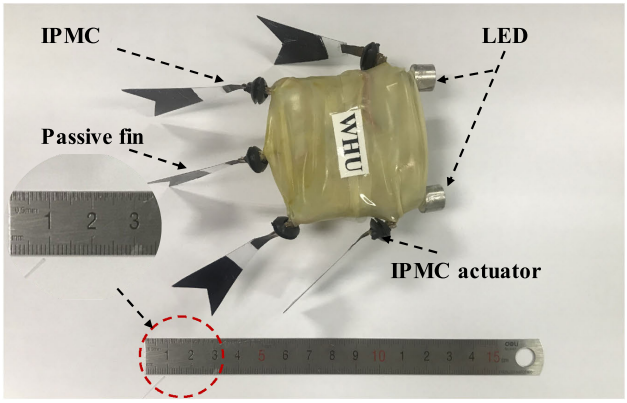

FIGURE 1. Prototype of the miniature robotic turtle, which contains the ultrasonic receivers, the IPMC, and passive fins.

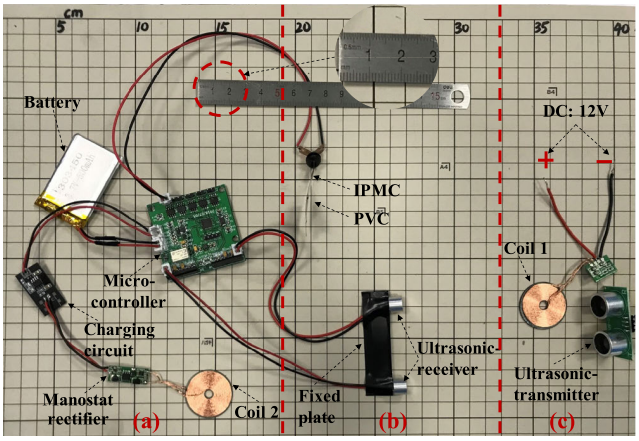

FIGURE 2. Onboard electronics of the robotic turtle system (a) internal parts of waterproof shell, (b) external parts of the shell, (c) the charging station.

TABLE 1. Technical specifications of the robotic turtle.

Items	Characteristics
Size ($L \times W \times H$)	~ 95 mm × 60 mm × 15 mm
Total mass	30 g
Control mode	Autonomous
Controller	STMicroelectronics, STM32F103T8U6
Power supply	500 mAh, 3.7 V, LiPo battery
Onboard sensors	ultrasonic sensors
Drive mode	H-bridge
Actuators	IPMC (0.2 mm) + PVC (0.2 mm)
Surface area of actuators	3 cm^2
Size of coils	$\Phi = 25$ cm
Operation time	~ 2 h
Maximum velocity	1.8 cm/s

A. SYSTEM SCHEMATICS

The schematic of the miniature robotic turtle with target tracking and wireless charging systems is shown in Fig. 3. The design depicts the control system (left of Fig. 3),

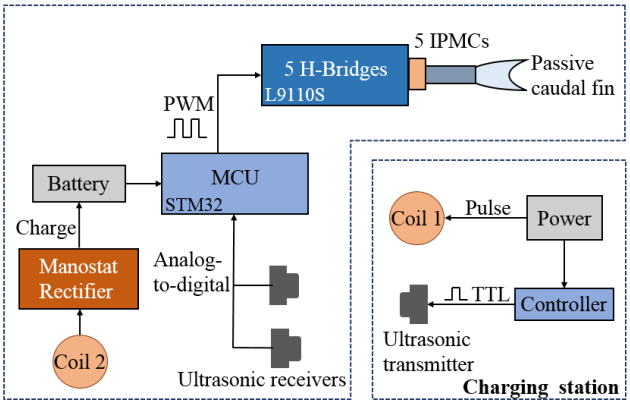

FIGURE 3. Schematic of the robotic turtle with target tracking and wireless charging systems.

an underwater charging station (right of Fig. 3) and a wireless charging system. The control system is composed of a power supply battery, a microcontroller unit (MCU), five H-bridge driving circuits, five IPMCs and passive fins, two ultrasonic receivers and a wireless charging receiving module (including rectifier and voltage regulator module circuits and a secondary coil). The underwater charging station is made up of a power source, a controller, a wireless charging module (including a rectifier circuit and a secondary coil) and an ultrasonic transmitter.

The electronic components of the miniature robotic turtle consist of the MCU (STM32F103T8U6, STMicroelectronics, Sweden), two ultrasonic receivers (EU10AIF40H07T/R, E-Sound, Co., Ltd., China), a battery (303450, 500 mAh, 3.7 V, LiPo, China), coil 2, and the IPMC actuator. The IPMC actuator is made from an acid polymer (Nafion 117, Du Pont Co., USA), which is chemically plated with platinum on both sides. Compared to other smart materials, the IPMC actuator is superior for its faster response and lower driven voltage.

The system workflow is as follows. First, we power up the Printed Circuit Board system of the robotic turtle. The MCU initiates Pulse Width Modulations and outputs square wave signals to drive the IPMC by the H-bridge circuit. The MCU has ten wave output ports, and every two ports control a H-bridge circuit to drive an IPMC to swing left or right. The five groups of IPMC-driven fins can achieve the desired movements through different instructional combinations, including going straight, turning left or turning right. An ultrasonic transmitter placed at the underwater charging station transmits ultrasonic waves. Then two ultrasonic receivers placed in the two eyes of the miniature turtle receive the ultrasonic waves. These received ultrasonic signals are transmitted to the MCU after A/D conversion. Based on which "eye" receives the ultrasonic signal earlier, the MCU changes the swing combination of the IPMC fins by adjusting the output waveform. Coil 1 is placed directly in front of the ultrasonic transmitter as the charging target and coil 2 is placed at the bottom of the miniature robotic turtle. When the two coils come close to each other and produce an induction, the robotic turtle can charge itself. This paper focuses on target tracking and wireless charging. So in order to get smaller and lighter micro robots, we don't put extra sensors on this robot turtle.

B. TARGET TRACKING METHOD

There are a variety of target tracking methods that can be implemented in the system design, such as those based on radio waves, sound waves, light sensing and infrared sensing. However, due to the high attenuation of these signals in water, marine robots are subject to greater environmental disturbances. For this reason, we adopt the ultrasonic signal, which has little attenuation in water, to achieve target tracking.

Two ultrasonic receivers are mounted side-by-side on the head of the micromachine turtle as "eyes" and the ultrasonic transmitter is employed as the target for the robotic turtle to track. The ultrasonic transmitter can transmit ultrasonic waves with a 40 kHz beam, and the effective transmission distance of the ultrasonic waves is 0.3 to 3 m. Additionally, the effect of ultrasound on marine life can be ignored.

As shown in Fig. 4, after two ultrasonic receivers receive the sound wave transmitted by the ultrasonic transmitter, the robot's control algorithm can identify whether the "eye" on the left or the "eye" on the right receives the sound wave first. If the ultrasonic receiver on the left receives the sound wave first, it means that the robot is on the right side compared with the correct heading, and then this algorithm will control the robot to turn left. Instead, the algorithm will control the robot to turn right. Through many experiments and debugging, if $\beta > \pm$ (5-10)°, and $< 80°$, the control algorithm can identify whether the robot is left or right relative to the correct heading. If $\beta < \pm$ (5-10)°, it is considered that the robot's heading is right facing the ultrasonic transmitter. If $\beta > 80°$ (the heading is beyond the receiving range of the ultrasonic receiver), the control algorithm will control the robot to rotate until the ultrasonic receivers receive the ultrasonic wave.

III. PERFORMANCE EVALUATION OF KEY COMPONENTS

A. SWINGING PERFORMANCE OF AN INDIVIDUAL IPMC

The swinging performance of the IPMC is the key to achieve the desired driving level of the robotic turtle. The tip deflection of a single IPMC actuator is measured for its performance under a square wave drive signal. Fig. 5 shows the dynamic process of measuring an IPMC actuator driven by a square wave signal. The CMOS camera (C13440-20CU, Hamamatsu, Japan) captures images of the IPMC at different times during each swing round-trip-time.

Fig. 6 shows the process of the IPMC when it swings one round-trip-time at the right of the center line with a oscillation period of approximately 1.87 s. In this timeframe, the IPMC is at rest at 0 s and attains its rightmost deflection at 0.78 s, after which it returns to rest at its center line at 1.87 s. The swing displacement δ of the tip of the IPMC at each moment in consecutive periods is measured, where the δ value is converted from the pixel value to the displacement value. The

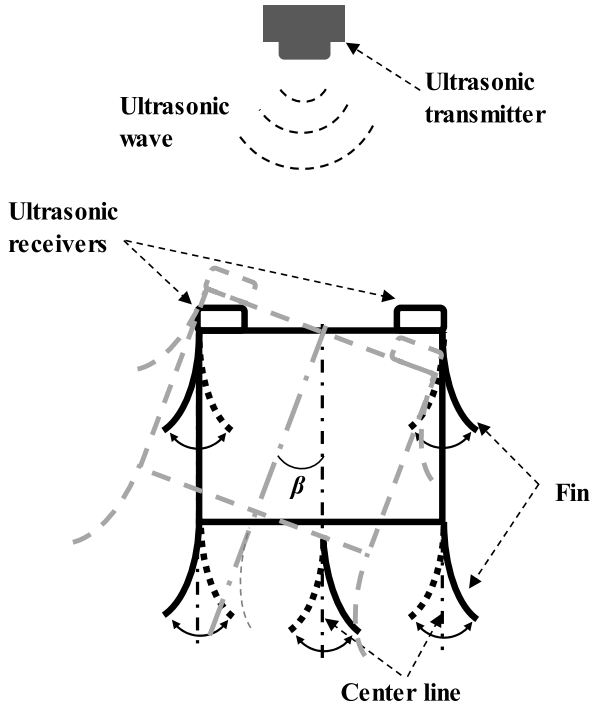

FIGURE 4. Schematic of the target tracking method.

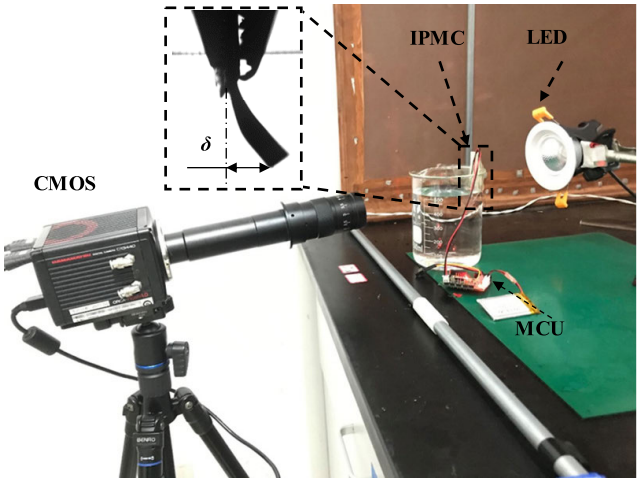

FIGURE 5. IPMC swing motion observed by the CMOS camera.

amplitude of the left and right swing of the IPMC is about 4 mm. Its swing frequency is consistent with the frequency of the square wave.

B. SWING PERFORMANCE OF THE IPMC WITH A PASSIVE FIN

The IPMC actuators are further covered by passive PVC fins to enhance propulsion. To test the kinematics of the IPMC and verify the proposed design method of the passive fin, the IPMC with a 30 mm PVC is placed in the water and continuously photographs by a single-lens reflex camera (EOS-1D X Mark II, CANON, Japan). Because of the light

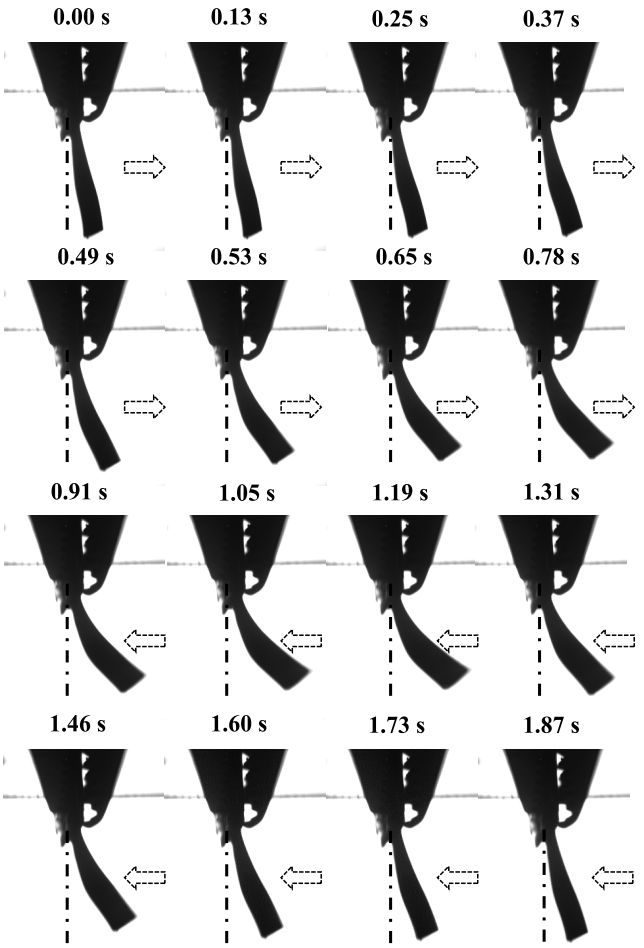

FIGURE 6. Capturing IPMC swing periodogram by the CMOS camera.

weight of passive fin, its influence on the propulsive force generated by the actuators can be ignored.

Fig. 7(a) depicts the experimental results of the flapping motion of the actuator in water, in which the flapping amplitude of the active body is 25 mm and the swing round-trip-time is approximately 1.83 s. It shows a complete flapping cycle in which twelve frames are captured respectively. In each frame, the white arrow denotes the direction of flapping. By comparing the arrow direction and time of Fig. 6 and Fig. 7(a), it can observe that the bending of the IPMC with passive fin is visible, and the swing trend in the experiment is well agreed with that of the IPMC without passive fin (Fig. 6).

To quantitatively measure and analyze the motion errors between the IPMC and the IPMC with passive fin, four frames at time 0 s, 0.5 s, 1 s and 1.5 s are selected. By measuring the vertical distances between the midline and the end of IPMC, the center and end of passive fin, we obtain the errors.

Fig. 7(b) depicts the error between the distance from 3 points on the IPMC with passive fins to the centerline and the distance from the corresponding point of the imaginary extension line of the IPMC without passive fins to the centerline. We name this error as lateral deflection error. In addition,

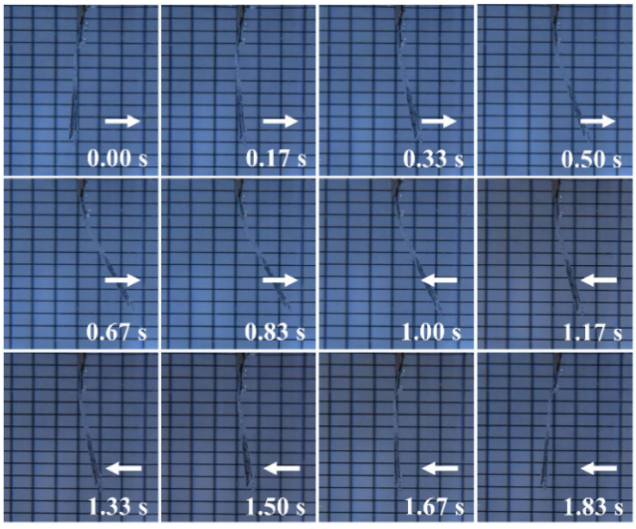

(a)

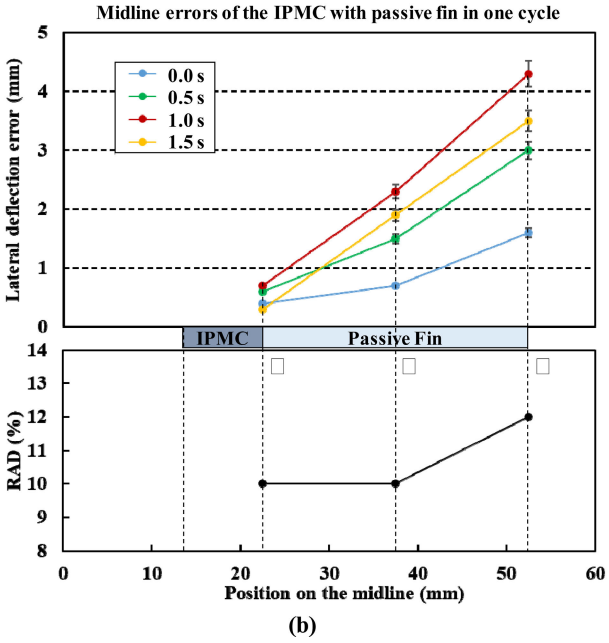

(b)

FIGURE 7. (a) Swing motions of the IPMC with a passive fin observed by a SLR camera and (b) midline deflection errors compared to the IPMC without passive fin.

these 3 points are the end of IPMC (I), the center (II) and end of passive fin (III). The distances are measured manually with the pixel tool. In Fig. 7(b), four curves represent the errors of 3 points in four moments in a flapping cycle. The maximum error is approximately 4.2 mm at the point III at 1 s. The maximum distance measured manually at the point III is 26 mm; therefore, the relative deviation is about 16% (4.2/26 = 16%). The lateral deflection error at 1.5 s is larger than that at 0.5 s, because the fin is swung by inertia toward the centerline from 1 s to 1.5 s. Averaging these relative deviations of 0 s, 0.5 s, 1 s and 1.5 s at three different points, we obtain the relative average deviation (RAD): 10% (I), 10% (II), and 12% (III) corresponding, respectively. Therefore, the largest RAD appears at the end of passive fin.

Overall, IPMC is a new kind of smart material. They consist of one proton exchange mat layer and two metal electrodes on both sides. The structure of IPMC is similar to a ''sandwich'', When a DC voltage difference is applied on both ends of the electrodes, IPMC can generate mechanical bending in the direction of the anode [30]. The method of design IPMC actuator can be used to guide this type of robot fish driven by smart actuators. The error may be attributed to some factors, such as the response time of IPMC and the resistance of swing in water caused by the increase of fin surface area. As a result, it may not be able to strictly follow every time step of the IPMC without passive fin. It confirms that the actuator can vibrate along its fundamental mode, which is necessary for the miniature robotic turtle to move at the desired trajectories.

C. EVALUATION OF THE WIRELESS CHARGING MODULE

This section explains the power supply and charging conversion method of the designed robot turtle battery, as well as the performance index of the designed wireless charging. Fig. 8(a) shows wireless charging and operation switching system schematic of the robot turtle by the electromagnetic microrelay. The normal closing switch of electromagnetic microrelay indicates that the battery (V_{Battery}) supplies power to the circuit board (V_{Board}) to make the robot operating. When the position deviation between coil 2 and coil 1 is within the effective charging distance, the wireless charging receiving module will output 5 V voltage through rectifier and voltage stabilizing. One way current is connected with the electromagnet controlling single-pole double-throw (SPDT) switch of the electromagnetic microrelay, and the other is connected with the positive charge (V_{Charge}) for the battery. When the electromagnet of the electromagnetic relay works, that is, the normal opening switch of the electromagnetic microrelay closes, the battery will be charged and the robot turtle will not operate.

In Fig. 8(b), coil 1 and coil 2 are the primary and secondary coils, respectively. A 3.7 V voltage specification lithium ion battery is used as the power source, which requires an effective charging voltage of 4.2 V. In Fig. 8(b), d_{ex} and d_{ey} denote the effective charging distance between the centers of the two coils in the x and y directions, respectively.

It can be seen that when the distance in the y direction between coil 1 and coil 2 is between 0 and 20 mm, an effective output voltage ($\geq$4.2 V) can be obtained. Similarly, when the distance in the x direction between the centers of coil 1 and coil 2 is between 0 and 8 mm, an effective output voltage ($\geq$4.2 V) is obtained.

IV. SYSTEM EVALUATION

The robotic turtle is employed with five fins driven by five IPMCs with passive fins to enable forward and turning motions. Schematics of the different motions are shown in Fig. 9. Correspondingly, Fig. 10 shows the square wave signals that drive the IPMC fins. The square wave signal has a period of 2 s and a voltage amplitude of 3.3 V. The

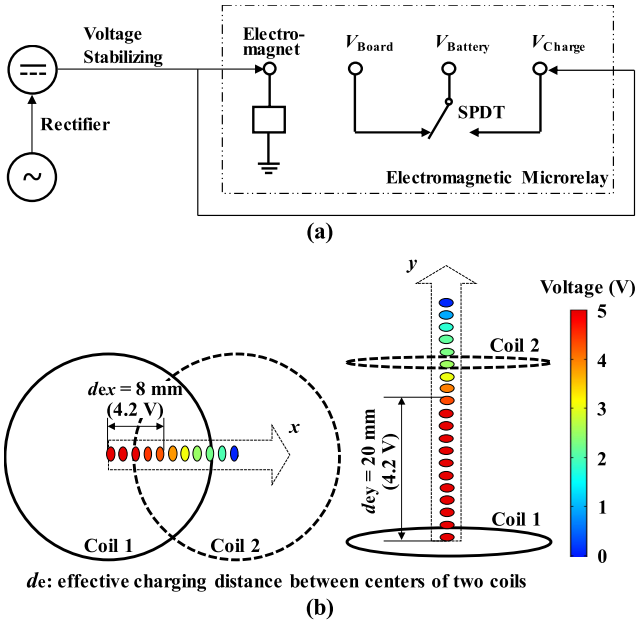

FIGURE 8. (a) Circuit system of wireless charging of the robot turtle and (b) effective output voltage of the electromagnetic induction wireless charging station.

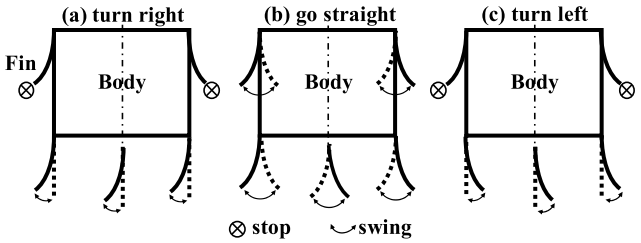

FIGURE 9. Actuator motions of moving forward and making turns: (a) turning left (b) moving forward (c) turning right.

square waves shown in Fig. 10(a), (b) and (c) indicate driving signals for motion of right turn, moving forward and making a left turn, respectively. Additionally, the right turn signal in Fig. 10(a) and the left turn signal in Fig. 10(c) are symmetrical.

A. TRACKING PERFORMANCE

For the target tracking and wireless charging systems, the charging station is designed to guide the robotic turtle to coil 1 by using the ultrasonic transmitter when the robotic turtle needs to charge. An ultrasonic transmitter is installed 5 cm directly behind coil 1 in the underwater charging station, which is used as the transmitter for the target tracking. Two receivers on the robotic turtle can capture the ultrasonic signal emitted by the transmitter. By comparing the time order of the signals received by the two receivers, the robotic turtle can change its motion by turning right, going straight or turning left. An angle threshold value is set for the motion control of the robotic turtle ($\pm 3°$ used in this paper). If the angle between normals of the two receivers is larger than

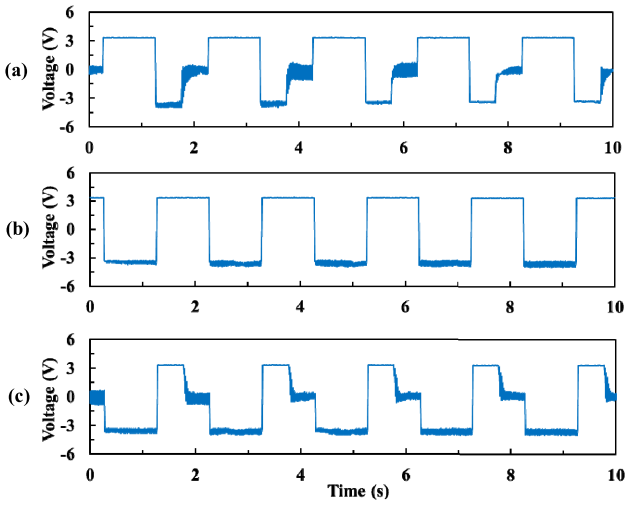

FIGURE 10. Drive signals for the IPMCs (a) one direction to the left (b) swing left and right (c) one direction to the right.

the threshold value, the robotic turtle will change swimming directions. Otherwise, the robotic turtle will go straight. When the left sensor receives the ultrasonic signal first, the robotic turtle turns left; otherwise, the robotic turtle will turn right. Thus, the robotic turtle can swim to the charging station automatically with the target tracking system.

The video tracking the experimental process is intercepted into images with a time interval of 2 seconds, which is captured by through the video editing software, as shown in Fig. 11. The robotic turtle turns left until it faces the ultrasonic transmitter, and then it swims straight to coil 1. It takes 22 s for the robotic turtle to swim from the starting point to coil 1 with an initial distance of 30 cm and an angle of 60°.

By manually measuring the pixel distance and scale conversion of two adjacent frames (the time interval is 2 seconds), the speed of the robotic turtle at each time is calculated. The tracking performance of the robotic turtle with different initial angles is measured as shown in Fig. 12. The initial swimming directions of the robotic turtle are 80°, 50°, 20° and −30° from the horizontal direction. The trajectory of the head center is displayed with dotted lines. The maximum swimming speed of the robotic turtle is about 1.8 cm/s. It takes between 7 s and 9 s for the turtle to speed up to 1.8 cm/s. When the initial distance is 30 cm and the initial angles are 80°, 50°, 20° and −30°, the target tracking times for the robotic turtle are 38.4 s, 33.6 s, 27.2 s, and 32.0 s, respectively.

B. CHARGING EFFICIENCY

The autonomous wireless charging performance is evaluated using the initial angles selected from the tracking experiments. As shown in Fig. 13, the horizontal distance (d) between coil 2 disposes in the robotic turtle and coil 1 in the charging station are detected when the robotic turtle is being wirelessly charged. When d is within 8 mm, the robotic turtle can be charged effectively (as indicated in Fig. 8). Experimen-

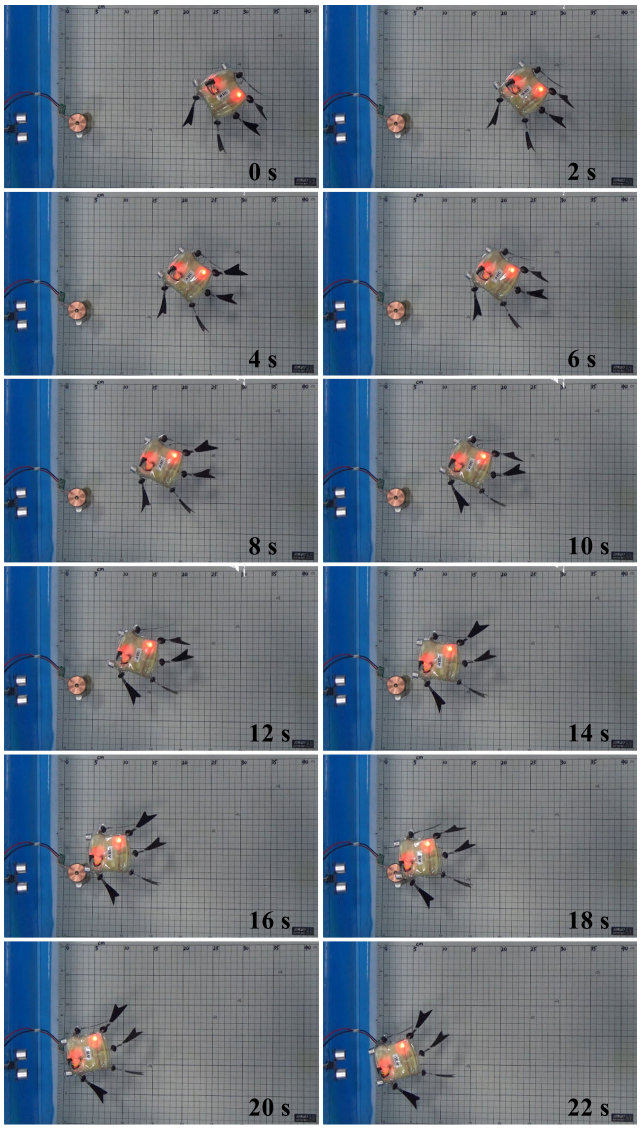

FIGURE 11. Ultrasonic tracking experiments: the initial distance between the robotic turtle and the charging station is 30 cm, and the initial swimming direction is 60° from the horizontal direction.

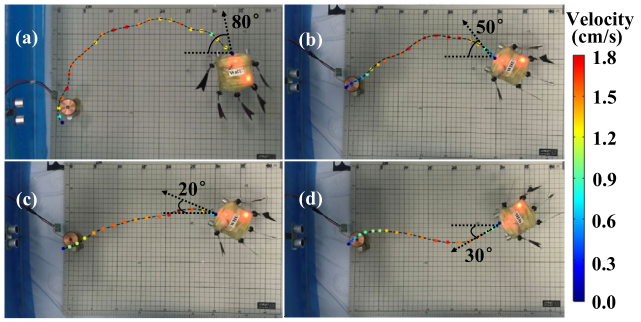

FIGURE 12. Ultrasonic tracking experiments of different initial swimming directions.

tal results on the success of tracking, the success of wireless charging, and the charging times are summarized in Fig. 14. On average, the result indicates that the tracking reliability is 85% (34/40 = 85%), with the initial angles playing a

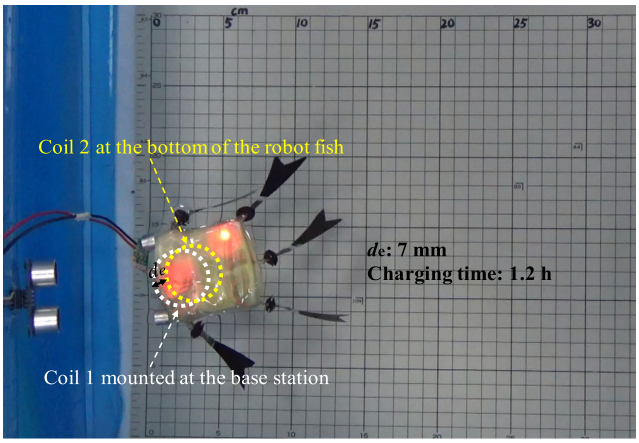

FIGURE 13. Wireless charging experiments.

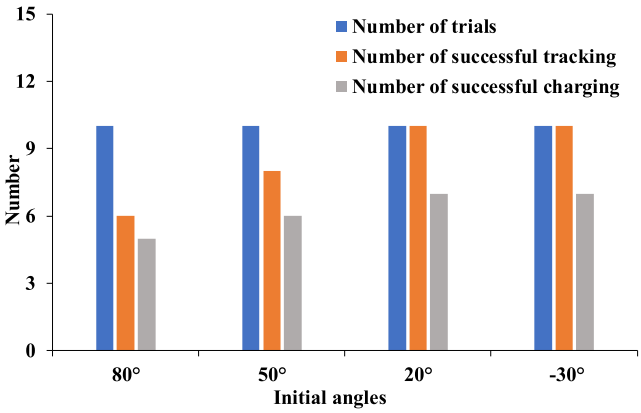

FIGURE 14. Results of the autonomous wireless charging.

central role on the tracking success. Specifically, when the initial angle is set below 50°, the tracking has an accuracy of 93% (28/30 = 93%). In contrast, when the initial angle is higher than 50°, the tracking is less reliable. Fig. 14 also demonstrates that not all successful tracking events lead to successful charging.

On average, the success rate of charging with successful tracking is 73% (25/34 = 73%). It is reasonable to suggest from these data that while larger initial angles may hinder the tracking process, they have no significant effect on the charging success rate. Furthermore, experiments show that the underwater wireless charging time averages 1.2 h. Moreover, after a full charge, the battery can continue to power the robot for about 3 h (the turtle can swim up to 194 meters) without wireless charging.

V. CONCLUSION

In this paper, a miniature robotic turtle with target tracking and wireless charging functions was designed. The robot used five fins driven by IPMCs to move forward and turn, and two ultrasonic receivers acted as eyes for tracking. Our target tracking approach is only based on the time order of the sonic wave reaching two ultrasonic receivers. Specifically,

the controller commanded the robotic turtle to approach the underwater station via target tracking. When the robotic turtle reached its minimum power supply, it could be able to wirelessly charge itself. Further, this system was able to extend the limits of its initial angles. In the first experiment, we systematically varied the initial angles of the robotic turtle toward the underwater station to assess its impact on target tracking time and swimming time. Results indicated that an initial angle of 20° was preferable, providing both rapid and effective tracking. In the second experiment, we carried out 40 automatic wireless charging experiments of the robotic turtle in four different initial positions. The autonomous tracking error was determined to have a 6 mm displacement radius, and the success rate of charging was found to be greater than 73%. The results of this work provide practical methods and cases for solving the problem of short working time of micro underwater vehicle. In summary, the robotic turtle developed in this paper represents a noteworthy advance in the field of autonomous marine robotics. We anticipate that insights gained from these studies will inform the design of new underwater technologies with unique features.

REFERENCES

[1] X. Guo, S. Ma, B. Li, and Y. Fang, "A novel serpentine gait generation method for snakelike robots based on geometry mechanics," *IEEE/ASME Trans. Mechatronics*, vol. 23, no. 3, pp. 1249–1258, Jun. 2018.

[2] D. Li, P. Wang, and L. Du, "Path planning technologies for autonomous underwater Vehicles–A review," *IEEE Access*, vol. 7, pp. 9745–9768, 2019.

[3] A. Li, L. Ye, J. Yanqing, L. Yueming, C. Jian, and H. Jiayu, "Soft-switching proximate time optimal heading control for underactuated autonomous underwater vehicle," *IEEE Access*, vol. 7, pp. 143233–143249, 2019.

[4] J. Cao, D. Lu, D. Li, Z. Zeng, B. Yao, and L. Lian, "Smartfloat: A multimodal underwater vehicle combining float and glider capabilities," *IEEE Access*, vol. 7, pp. 77825–77838, 2019.

[5] H. Wang, C. Mi, Z. Cao, J. Zheng, Z. Man, X. Jin, and H. Tang, "Precise discrete-time steering control for robotic fish based on data-assisted technique and Super-Twisting-Like algorithm," *IEEE Trans. Ind. Electron.*, vol. 67, no. 12, pp. 10587–10599, Dec. 2020.

[6] J. Yu, Z. Wu, X. Yang, Y. Yang, and P. Zhang, "Underwater target tracking control of an untethered robotic fish with a camera stabilizer," *IEEE Trans. Syst., Man, Cybern. Syst.*, early access, Jan. 13, 2020, doi: 10.1109/TSMC.2019.2963246.

[7] F. Xie, Z. Li, Y. Ding, Y. Zhong, and R. Du, "An experimental study on the fish body flapping patterns by using a biomimetic robot fish," *IEEE Robot. Autom. Lett.*, vol. 5, no. 1, pp. 64–71, Jan. 2020.

[8] W. Wang, D. Gu, and G. Xie, "Autonomous optimization of swimming gait in a fish robot with multiple onboard sensors," *IEEE Trans. Syst., Man, Cybern. Syst.*, vol. 49, no. 5, pp. 891–903, May 2019.

[9] T. Fukuda, H. Hosokai, and I. Kikuchi, "Distributed type of actuators by shape memory alloy and its application to underwater mobile robotic mechanism," in *Proc. IEEE Int. Conf. Robot. Autom.*, Cincinnati, OH, USA, vol. 2, May 1991, pp. 1316–1332.

[10] S. Guo, T. Fukuda, and K. Asaka, "A new type of fish-like underwater microrobot," *IEEE/ASME Trans. Mechatronics*, vol. 8, no. 1, pp. 136–141, Mar. 2003.

[11] L. Fearing, "Micro structures and micro actuator for implementing submillimeter robots," *Precision Sensors, Actuators and Systems*. Dordrecht, The Netherlands: Springer, 1992, pp. 39–72.

[12] T. Fukuda, A. Kawamoto, and F. Arai, "Steering mechanism of underwater micro mobile robot," in *Proc. IEEE Int. Conf. Robot. Automat.*, vol. 1, May 1995, pp. 363–368.

[13] M. Mojarrad and M. Shahinpoor, "Biomimetic robotic propulsion using polymeric artificial muscles," in *Proc. Int. Conf. Robot. Autom.*, Albuquerque, NM, USA, Apr. 1997, pp. 2152–2157.

[14] S. Guo, T. Fukuda, N. Kato, and K. Oguro, "Development of underwater micro robot using ICPF actuator," in *Proc. IEEE Int. Conf. Robot. Automat.*, Leuven, BEL, May 1998, pp. 1829–1834.

[15] M. Shahinpoor, "Conceptual design, kinematics and dynamics of swimmingrobotic structures using ionic polymeric gel muscles," *Smart Mater. Struct.*, vol. 1, no. 1, p. 91, 1992.

[16] K. Mohseni, "Pulsatile vortex generators for low-speed maneuvering of small underwater vehicles," *Ocean Eng.*, vol. 33, no. 16, pp. 2209–2223, Nov. 2006.

[17] X. Tan, D. Kim, N. Usher, D. Laboy, J. Jackson, A. Kapetanovic, J. Rapai, B. Sabadus, and X. Zhou, "An autonomous robotic fish for mobile sensing," in *Proc. IEEE/RSJ Int. Conf. Intell. Robots Syst.*, Beijing, China, Oct. 2006, pp. 5424–5429.

[18] Z. Chen, S. Shatara, and X. Tan, "Modeling of biomimetic robotic fish propelled by an ionic polymer-metal composite caudal fin," *IEEE-ASME Trans. Mechatronics*, vol. 15, no. 3, pp. 448–459, 2009.

[19] M. Aureli, V. Kopman, and M. Porfiri, "Free-locomotion of underwater vehicles actuated by ionic polymer metal composites," *IEEE/ASME Trans. Mechatronics*, vol. 15, no. 4, pp. 603–614, Aug. 2010.

[20] Y.-C. Chang and W.-J. Kim, "Aquatic ionic-polymer-metal-composite insectile robot with multi-DOF legs," *IEEE/ASME Trans. Mechatronics*, vol. 18, no. 2, pp. 547–555, Apr. 2013.

[21] M. Li and S. Guo, "A wireless biomimetic underwater microrobot for a father-son robot system," in *Proc. IEEE Int. Conf. Mechatronics Autom.*, Harbin, China, Aug. 2016, pp. 392–397.

[22] M. Li, "Development of a biomimetic underwater microrobot for a father-son robot system," *Microsyst. Technol.*, vol. 23, no. 4, pp. 849–861, 2016.

[23] B. Gao and S. Guo, "Development of an infrared ray controlled fish-like underwater microrobot," in *Proc. IEEE Int. Conf. Autom. Logistics*, Aug. 2010, pp. 150–155.

[24] L. Chen, S. Wang, H. Hu, D. Gu, and L. Liao, "Improving localization accuracy for an underwater robot with a slow-sampling sonar through graph optimization," *IEEE Sensors J.*, vol. 15, no. 9, pp. 5024–5035, Sep. 2015.

[25] R. K. Katzschmann, J. DelPreto, R. MacCurdy, and D. Rus, "Exploration of underwater life with an acoustically controlled soft robotic fish," *Sci. Robot.*, vol. 3, no. 16, Mar. 2018, Art. no. eaar3449.

[26] W. Wang and G. Xie, "Online high-precision probabilistic localization of robotic fish using visual and inertial cues," *IEEE Trans. Ind. Electron.*, vol. 62, no. 2, pp. 1113–1124, Feb. 2015.

[27] R. Itoh, Y. Sawahara, T. Ishizaki, and I. Awai, "Wireless power transfer to moving ornamental robot fish in aquarium," in *Proc. IEEE 3rd Global Conf. Consum. Electron. (GCCE)*, Tokyo, Japan, Oct. 2014, pp. 459–460.

[28] K. Abdelnour, A. Stinchcombe, M. Porfiri, J. Zhang, and S. Childress, "Wireless powering of ionic polymer metal composites toward hovering microswimmers," *IEEE/ASME Trans. Mechatronics*, vol. 17, no. 5, pp. 924–935, Oct. 2012.

[29] P. Phamduy, J. Cheong, and M. Porfiri, "An autonomous charging system for a robotic fish," *IEEE/ASME Trans. Mechatronics*, vol. 21, no. 6, pp. 2953–2963, Dec. 2016.

[30] S. Tadokoro, S. Yamagami, T. Takamori, and K. Oguro, "Modeling of Nafion-Pt composite actuators (ICPF) by ionic motion," *Proc. SPIE*, vol. 3987, pp. 92–102, Jun. 2000.

QIMENG SUN (Member, IEEE) was born in Xuzhou, China, in 1994. He received the B.Eng. degree in mechatronics engineering from the Nanjing Institute of Technology, Nanjing, China, in 2016, and the M.Eng. degree in mechanical engineering from Wuhan University, Wuhan, China, in 2019.

He is currently a Researcher with China Electronics Technology Group Corporation. His research interests include ultrasound tracking, mechanical structure design, and signal processing, including audio and video signals.

JINZHE HAN was born in Xiantao, China, in 2000. He is currently pursuing the bachelor's degree with the School of Power and Mechanical Engineering, Wuhan University. His research interests include mechanical structure design and the reliability of electronic products.

HUI LI (Senior Member, IEEE) received the B.E. degree from the Huazhong University of Science and Technology, Wuhan, China, in 1999, and the Ph.D. degree in electrical and computer engineering from the National University of Singapore, Singapore, in 2007.

He is currently a Professor with Wuhan University, China. His research interests include the design of micro/nanoelectromechanical systems and the reliability of electronic products.

SHENG LIU (Fellow, IEEE) received the B.E. degree from the Nanjing University of Aeronautics and Astronautics, Nanjing, China, in 1983, and the Ph.D. degree in mechanical engineering from Stanford University, USA, in1992.

He is currently a Professor with Wuhan University, China. His research interests include manufacturing process modeling and reliability assessment. He is the Fellow of the ASME. He has achieved systematic original research output in the areas of electronic manufacturing and stability. He has received the White House/NSF Presidential Faculty Fellows Award in 1995 and the First Prize for Technological Invention of CIE in 2018.

SHENGNAN SHEN (Senior Member, IEEE) received the B.E. degree from the Harbin Institute of Technology, Weihai, China, in 2005, and the Ph.D. degree in mechanical and aerospace engineering from Nanyang Technological University, Singapore, in 2013.

She is currently an Associate Professor with Wuhan University, China. Her research interests include precision mechanical design, and the design and applications of high precision positioning control.

YUNFAN ZHANG (Member, IEEE) was born in Huanggang, China, in 1994. He received the B.Eng. degree from Hunan University, Changsha, China, in 2016, and the M.Eng. degree in mechanical engineering from Wuhan University, Wuhan, China, in 2019, where he is currently pursuing the Ph.D. degree.

His research interests include MEMS reliability and wearable flexible circuits.

JIAZHENG SHENG was born in Xinyang, China, in 1994. He received the B.Eng. degree from the Henan University of Technology, Zhengzhou, China, in 2016, and the M.Eng. degree in mechanical engineering from Xiamen University, Xiamen, China, in 2019. He is currently pursuing the Ph.D. degree with Wuhan University.

His research interest includes FPCB processing technology.